DOI. No. 10.1109/MAES.2016.150155

Feature Article:

Vision-Based UAV Collision Avoidance with 2D Dynamic Safety Envelope

***Yang Lyu, Quan Pan, Chunhui Zhao, Yizhai Zhang, Jinwen Hu*, Northwestern Polytechnical University, Xi'an, China**

INTRODUCTION

Because of low-cost, high-autonomy, and super-flexibility, unmanned aerial vehicles (UAVs) have the potential to be an excellent mobile platform in many military applications. Recently, with the advances of dynamics [1], navigation [2], and sensors [3], [4], more civilian applications have been realized on the UAVs, such as surveillance [5], aerial photography [6], search and rescue [7], and others. For all of these applications within civilian airspace, one critical technical requirement is the integration of UAVs into the current civilian air-traffic-control system. However, the use of UAVs further increases the density of the civilian airspace that is already crowded with manned aerial vehicles. In order to guarantee safety, the "Sense and Avoid" (SAA) is considered critical for UAVs used in civilian airspace [8]. SAA requires that the UAV system is not only capable of detecting the potential collision objects, but also able to implement the necessary collision avoidance maneuvers.

Many SAA prototypes [9]–[13] have been reported recently containing various sensors. The sensors are generally divided into two categories: cooperative sensors, such as traffic collision avoidance system (TCAS) Light (LIght) [9] and Automatic Dependent Surveillance-Broadcast [10], and uncooperative sensors such as camera [11], radar [12], or LIght Detection And Radar [13]. The SAA prototypes usually use one sensor or a combination of multiple sensors [14]. For the non-cooperative intruder, the uncooperative sensors are very useful because communications between the host UAV and the intruder are not available. Among all of the uncooperative sensors, a camera has great advantages over the others as it is low-cost and light-weight but provides rich information, making it an attractive option, especially for small, unmanned aerial vehicles with limited payload capacity. Although the use of a camera is attractive, vision-based SAA of UAVs is challenging for two reasons. First, the vision-based intruder sensing methods for SAA, e.g., visual tracking, are not trivial, especially when the intruder is small and dim in the image. Second, an onboard camera cannot measure the distance between the host UAV and the intruders [15], and this distance information is extremely important for traditional obstacle avoidance methods, such as Rapidly-Exploring Random Tree [16], *A** [17], and others.

There have been many recent studies of sensing methods for vision-based SAA [18], [19], [20], [11], [21]. In [18], a morphological method is first used to highlight the small and dim intruder against the non-homogeneous background. A temporal filter using multi-frame information is then adopted to steadily detect and track the intruder. A frequency-domain method called regional phase correlation is proposed in [19]. [11] presents a vision-based detection system using a Graphics Processing Unit to fulfill the real-time computation requirement. In [21], a vision-based intruder detection system is realized by using five cameras to achieve wide field of view (FOV).

In order to achieve avoidance maneuver with vision information, many approaches are proposed to obtain the distance information or to perform avoidance without a requirement for distance information. For example, a laser-based range finder is used to directly measure the distance in [22] though this solution requires a higher UAV payload capacity. In [23], a target tracking filter estimates the distance as bearings-only target motion analysis. However, extra maneuvers of the host UAV are required to allow full observation for adequate performance of the filter. Other proposed methods are independent of the distance information. In [24], a vision-based SAA is implemented by maintaining a constant relative angle between the host UAV and the intruder. A similar approach is presented in [25] using visual predictive control. Although these methods are suitable to circumvent the need for distance information, they are unable to capture the collision threat if the intruder is approaching right along the pre-defined constant angle and thus, no collision avoidance maneuver is executed according to the controller design. In [26], a reactive collision avoidance algorithm is proposed based on the closest point of approach and the geometry of the intruder is obtained by a single vision sensor. In this algorithm, there are requirements for a priori knowledge such as the size of intruder, and such information is usually unavailable in SAA. In

Authors' current address: Y. Lyu, Q. Pan, C. Zhao, Y. Zhang, J. Hu, the Key Laboratory of Information Fusion Technology (LIFT), Ministry of Education; Y. Zhang is also with the Research Center for Intelligent Robotics, both departments are at Northwestern Polytechnical University, Youyi west road 127, Xi'an, Shaanxi 710072 China. The corresponding author is Y. Zhang at E-mail: zhangyizhai@nwpu.edu.cn. This work was supported in part by the National Natural Science Foundation of China under award 61473230 and 61403307 and the Chinese Fundamental Research Funds for the Central Universities award 3102014JCQ01070.
Manuscript received July 27, 2015, revised January 20, 2016, and ready for publication February 13, 2016.
Review handled by D. Maroney.

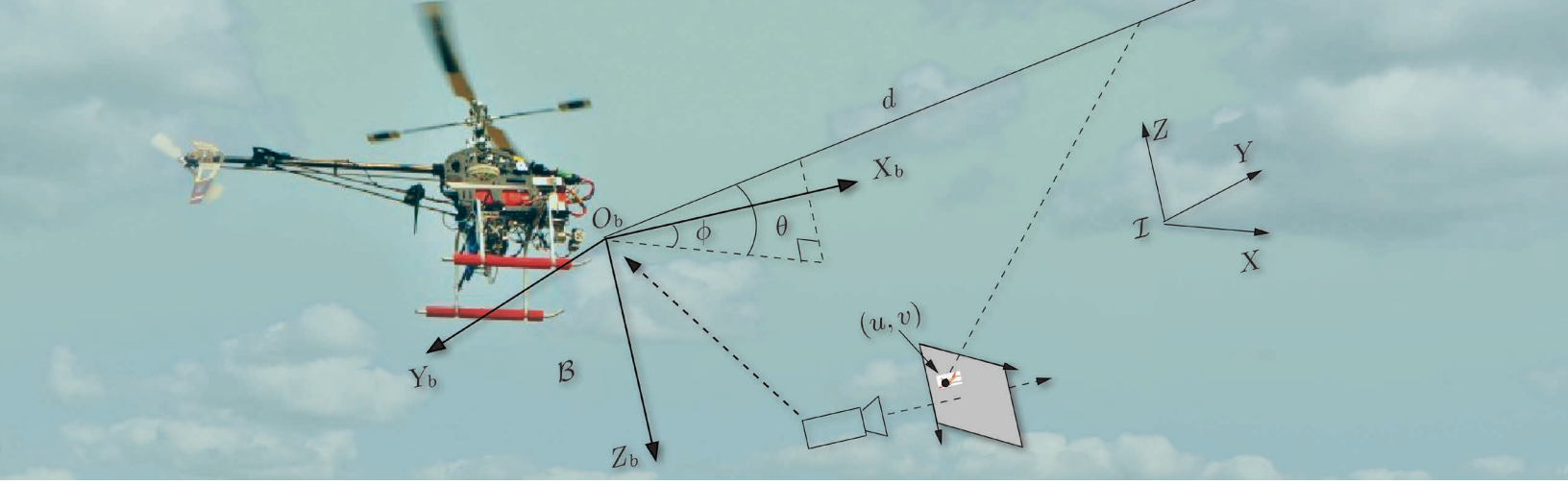

[27], a probabilistic-based collision risk estimation is proposed. By computing the collision probability for a predict trajectory, this method is suitable for the angle-only sensors that cannot provide accurate distance information.

In this article, we propose a novel, vision-based collision avoidance approach for UAVs. The intruder is assumed to be a non-cooperative object. A two-dimensional (2D) dynamic safety envelope is generated to capture the threat level of the intruder and guide the visual servoing controllers of the host UAV to avoid the intruder. To the best of our knowledge, this is the first proposal of the use of a dynamic safety envelope for vision-based SAA of UAVs. With the help of the dynamic safety envelope, the proposed approach is independent of the distance information and no extra maneuvers are needed. Thus, our approach provides a practical solution for the vision-based SAA of UAVs.

The rest of the article is organized as follows. In the section "SAA System and Coordinate System Definition", the overall SAA system and the coordinate system definition are described. The 2D dynamic safety envelope is then proposed in the section "Dynamic Safety Envelope". In the section "Visual Servoing Control Designs," two visual servoing controllers are designed to implement the avoidance maneuver and the returning maneuver of the SAA, separately. Finally, the simulation and experimental results are presented in the sections "Simulation Results", and "Experimental Results." The section called "Conclusion" presents the conclusions of this work.

SAA SYSTEM AND COORDINATE SYSTEM DEFINITION

Figure 1 shows the overall closed-loop system diagram of the SAA in our study. We consider the following procedures in the SAA. Initially, the host UAV follows a desired pre-defined trajectory $\mathcal{T}(t)$. Once an unequipped intruder is detected by the onboard, forward-facing camera, a 2D dynamic safety envelope is generated to continuously evaluate the threat level of the intruder. When the threat level becomes high and a collision may happen, two visual servoing controllers are used to avoid the intruder and then return to $\mathcal{T}(t)$, separately.

In this article, we adopt several assumptions. First, the SAA is assumed to be operating under middle-distance or long-distance conditions. Thus, the intruder is small in the image of the camera. We directly use the Close-Minus-Open and Hiden Markov Model (CMO-HMM) proposed in [11] for small target detection and tracking, so we only focus on the designs of the dynamic safety envelope and the visual servoing controls. Second, to simplify the SAA design, it is assumed that the roll angle of the host UAV is sufficiently small so that we can ignore the roll motion. This assumption is satisfied for the middle-distance or long-distance SAA where aggressive maneuvers by the host UAV are not needed. Third, we only consider the SAA in the FOV of the forward-facing camera because the camera is the only detecting sensor in our SAA system. The camera used in our study is a GoPro type wide FOV with 110° × 70°. Once the intruder leaves the field of view, it is assumed to pose no threat.

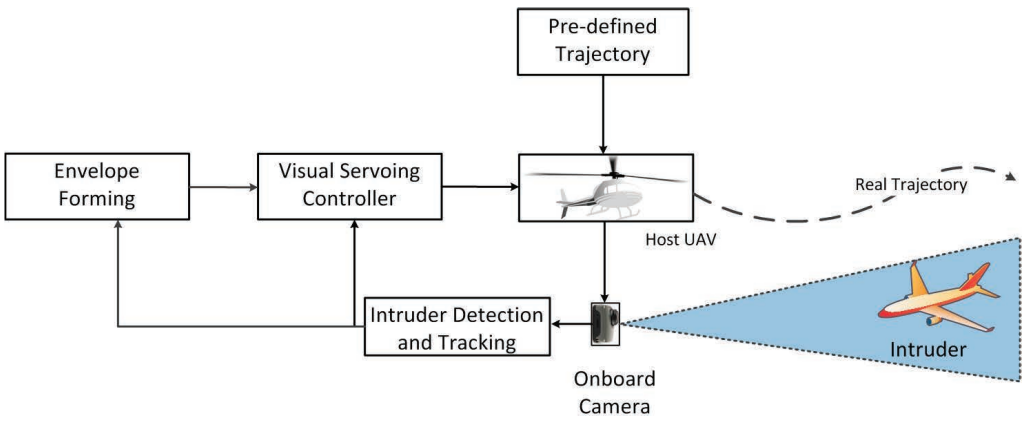

Figure 1.
Overall closed-loop system diagram.

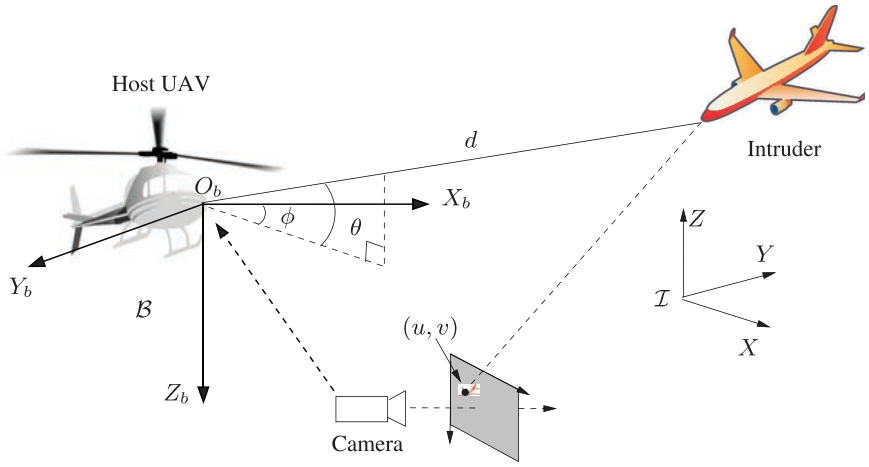

Figure 2.
SAA geometry.

In our SAA, the global inertial frame $\mathcal{I}(O, X, Y, Z)$ is defined with the Z-axis facing upwards. A camera is mounted on the head of the host UAV to detect a front potential intruder; see Figure 2. A UAV-fixed frame $\mathcal{B}(O_b, X_b, Y_b, Z_b)$ is defined with the X_b-axis facing forwards and the Z_b-axis pointing downwards. For simplicity, we assume the origin O_b of $\mathcal{B}$ is located at the camera center. Therefore, the camera's main axis coincides with X_b. The pinhole camera model is considered and the focal length of the camera is denoted as f. The camera pixel coordinate system is then defined with the origin at the top-left corner in the camera imaging plane; see Figure 2. W and H are the width and height of camera imaging plane, respectively. The field of view of the camera is denoted as $\mathcal{V}$. The CMO-HMM method provides only the intruder coordinates (u, v) in the camera imaging plane [11]. In order to facilitate SAA, the azimuth angle ϕ and the elevation angle θ of the intruder are used as the vision measurements [28]. The calculation from (u, v) to ϕ and θ is presented in [28].

We denote the distance between the host UAV and the intruder as d. d is not directly measured by the camera and, therefore, only the relative angles ϕ and θ can be used for collision avoidance control. For convenience, we define a vector $\mathbf{q} \coloneqq [\phi\ \theta]^T$. We also construct a 2D coordinate system $\mathcal{F}$ with the azimuth angle and the elevation angle as the two axes. Clearly, $\mathbf{q}$ is the position of the intruder in $\mathcal{F}$ and $[0\ 0]^T$ represents the forward direction of the host UAV. We define $\dot{\mathbf{q}}$ as the first-order derivative of $\mathbf{q}$ and $\dot{\mathbf{q}}$ shows how fast the intruder moves in $\mathcal{F}$.

DYNAMIC SAFETY ENVELOPE

PRELIMINARY

Inspired by the manned "see and avoid" process [29], we consider two similar rules in vision-based SAA of UAVs to determine a hazardous intruder:

- The intruder has the possibility to pass in front of the host UAV in a short time, and
- Observed from the host UAV, the intruder persists in the field of view.

The two rules define the situations when the collision avoidance maneuver of the host UAV becomes necessary. For the first rule, when the intruder is passing in front of the host UAV, there will be an interaction between the host UAV's and the intruder's trajectories. Without distance information available, this interaction is obviously dangerous. The second rule reveals that the aerial intruder usually flies with considerable speed and, therefore, it leaves the FOV quickly if it is not hazardous. On the contrary, the longer persistence of the intruder in the field of view increases the possibility that the intruder is approaching the host UAV. Similar observations based on pilots' experiences are presented in [29].

In this article, a 2D dynamic safety envelope $\mathcal{L}$ is proposed to analytically model the above two rules. The dynamic safety envelope is inspired by the concept of a "three-dimensional (3D) safety envelope" that represents the minimum separation zone around the host UAV [30]. However, the proposed dynamic safety envelope has two obvious differences. First, instead of the host UAV, $\mathcal{L}$ is intruder-centered. Second, $\mathcal{L}$ is built in the 2D coordinate system $\mathcal{F}$ rather than 3D space.

Remark 1: *The proposed dynamic safety envelope $\mathcal{L}$ is defined in $\mathcal{F}$ for two reasons. First, since no distance information is available, the dynamic safety envelope is difficult to build in 3D space, such as in $\mathcal{B}$. Second, the use of the azimuth and elevation angles is common in an omni-direction vision system. Thus, the proposed dynamic safety envelope can be easily extended to the omni-direction vision system, but the SAA strategies, such as the termination condition of the envelope evolution, shall be modified accordingly.*

DESIGN OF 2D DYNAMIC SAFETY ENVELOPE

When the intruder is initially detected, a circle envelope $\mathcal{O}$ is formed in $\mathcal{F}$ immediately. The center of $\mathcal{O}$ is at $\mathbf{q}$ and the initial radius of $\mathcal{O}$ is set as r_0. At this moment, the dynamic safety envelope is defined as $\mathcal{O}$, i.e., $\mathcal{L} = \mathcal{O}$. Afterwards, the center of $\mathcal{O}$ follows $\mathbf{q}$ and the radius can be written as

$$r_{i+1} = r_i + \varepsilon_0, \tag{1}$$

where r_i is the radius of $\mathcal{O}$ at the ith implementation time since the intruder is detected and ε_0 is a tuned parameter indicating that the collision threat is increasing as long as the intruder remains in the FOV.

For the dynamic safety envelope $\mathcal{L}$, we then consider two different cases:

Case 1: $\|\dot{\mathbf{q}}\| \le \varepsilon_1$ $\mathcal{L} = \mathcal{O}$; see Figure 3a. ε_1 is a threshold to determine the approaching state of intruder. This case represents the situation where the intruder moves slowly in $\mathcal{F}$ and we consider the intruder and host UAV are approaching to each other with considerable velocity.

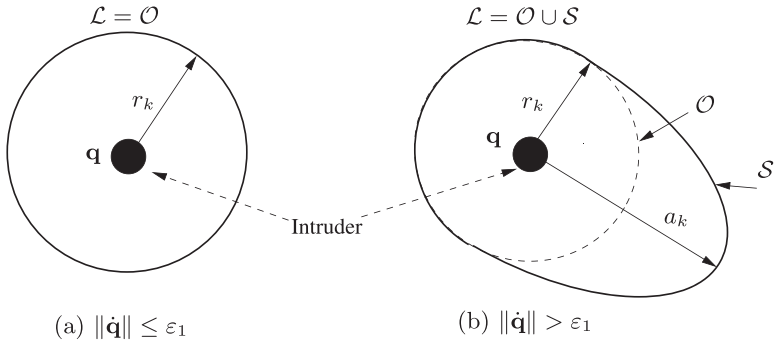

Figure 3.
2D dynamic safety envelope.

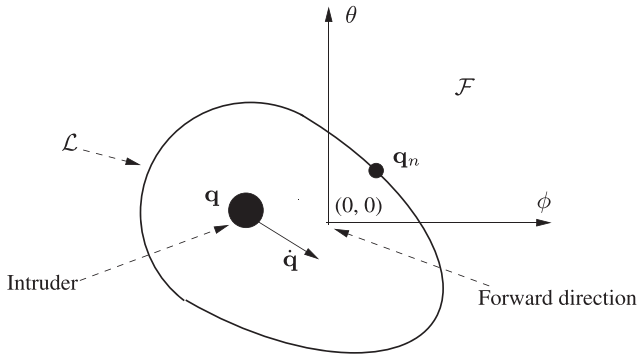

Figure 4.
Minimum avoidance maneuver on the dynamic safety envelope.

Case 2: $\|\dot{\mathbf{q}}\| > \varepsilon_1$ $\mathcal{L} = \mathcal{O} \cup \mathcal{S}$; see Figure 3b. In this case, $\mathcal{S}$ is a half ellipse. The orientation of the long axis of $\mathcal{S}$ aligns to the direction of $\dot{\mathbf{q}}$. The lengths of the long axis a_i and the short axis b_i of $\mathcal{S}$ are calculated respectively as

$$\begin{aligned} a_i &= r_i\left(1+\alpha\|\dot{\mathbf{q}}\|\right), \\ b_i &= r_i, \end{aligned} \tag{2}$$

where α is a tuned parameter that represents the position horizon prediction of the dynamic envelope evolution. It can be chosen according to the specific user safety requirement.

The dynamic safety envelope is eliminated when the intruder leaves the field of view, i.e., $\mathbf{q} \notin \mathcal{V}$.

Remark 2: *As defined above, the dynamic safety envelope $\mathcal{L}$ is constituted by only two components: $\mathcal{O}$ and $\mathcal{S}$. $\mathcal{O}$ is mainly used to evaluate the threat level of the intruder. Clearly, if the intruder persists in the FOV of host UAV, $\mathcal{O}$ increases to capture the hazard. $\mathcal{S}$ is used to compensate for the movement of the intruder.*

Although $\mathcal{L}$ is formed when the intruder is initially detected, the host UAV does not take any maneuver immediately. Initially, the intruder is just a potential hazard and may fly away. In our SAA, the intruder is confirmed as a severe threat and the host UAV starts to take avoidance maneuvers when two conditions are satisfied simultaneously: (1) the forward direction of the host UAV falls into the dynamic safety envelope, namely, $\begin{bmatrix}0 & 0\end{bmatrix}^T \in \mathcal{L}$; see Figure 4; (2) $r_i > r_{th}$ and r_{th} is a threshold. Only when the intruder remains in the FOV for enough time should a collision avoidance maneuver be taken.

Remark 3: *In this study, the SAA process is terminated when the intruder leaves the FOV because we assume the intruder is no longer a threat at this moment. We choose this criterion for several reasons. First, the wide view camera installed in the host UAV is already able to cover enough large forward FOV in most encountering scenarios. Second, since no other sensor is available, the termination criterion already maximizes the sensing capability. Third, as stated in [22], an intruder behind the UAV does not pose a threat as significant as a frontal intruder.*

A visual servoing control is used to implement the avoidance maneuver. Information from the dynamic safety envelope guides the visual servoing control. The objective of the visual servoing controller is to allow the forward direction $[0\ 0]^T$ of the host UAV to deviate from the dynamic safety envelope to avoid the intruder. To achieve a minimum maneuver, the nearest point $\mathbf{q}_n$ relative to $[0\ 0]^T$ on the $\mathcal{L}$ (see Figure 4) is calculated numerically. Thus, the ultimate objective of the visual servoing controller turns into moving $\boldsymbol{q}_n$ to the forward direction $[0\ 0]^T$.

VISUAL SERVOING CONTROL DESIGNS

VISUAL SERVOING CONTROL FOR INTRUDER AVOIDANCE MANEUVER

$\boldsymbol{q}_n$ is chosen as the visual feature $\boldsymbol{s}$ in the visual servoing control, namely $\boldsymbol{s} = \boldsymbol{q}_n$. Let us denote the spatial velocity of the host UAV as $\mathbf{V} = (\boldsymbol{v}^T, \boldsymbol{\omega}^T)^T$, where $\boldsymbol{v} = [v_x\ v_y\ v_z]^T$ is the instantaneous linear velocity vector and $\boldsymbol{\omega} = [\omega_y\ \omega_z]^T$ is the instantaneous angular velocity. Because we consider the long distance or middle distance SAA and the intruder is captured with point-like feature and in this situation, the UAV performs a slight maneuver rather than an aggressive maneuver. Therefore, zero roll motion is assumed and ω_x is omitted in the study. According to [31], [32], the relationship between the host UAV motion and visual feature motion in $\mathcal{F}$ is expressed as follows:

$$\dot{s}(t) = \mathbf{L}\mathbf{V}, \tag{3}$$

where $\mathbf{L}$ is the interaction matrix and in our SAA

$$\mathbf{L} = \begin{bmatrix} \dfrac{-\cos\phi\cos\theta}{d} & \dfrac{-\cos\phi\sin\theta}{d} & \dfrac{\sin\phi}{d} & -\cos\theta & 0 \\ \dfrac{\sin\theta}{d\sin\phi} & \dfrac{-\cos\theta}{d\sin\phi} & 0 & \dfrac{\sin\theta\cos\phi}{\sin\phi} & -1 \end{bmatrix}. \tag{4}$$

As stated above, the desired value of the feature $\boldsymbol{s}^*$ is the forward direction of UAV, namely, $\boldsymbol{s}^* = [0\ 0]^T$. The feature error between

$\boldsymbol{s}$ and $\boldsymbol{s}^*$ is $\boldsymbol{e} = \boldsymbol{s} - \boldsymbol{s}^*$. In addition, the term $\partial \boldsymbol{e}/\partial t$ is introduced to express the time variation of $\boldsymbol{e}$ due to the unknown intruder motion. Therefore, we obtain the error model as

$$\dot{\boldsymbol{e}} = \mathbf{L}\mathbf{V} + \frac{\partial \boldsymbol{e}}{\partial t}. \tag{5}$$

Equation 5 can be re-written as

$$\dot{\boldsymbol{e}} = \frac{1}{d}\mathbf{L}_v \boldsymbol{v} + \mathbf{L}_{\boldsymbol{\omega}} \boldsymbol{\omega} + \frac{\partial \boldsymbol{e}}{\partial t}, \tag{6}$$

where

$$\mathbf{L}_v = \begin{bmatrix} -\cos\phi\cos\theta & -\cos\phi\sin\theta & \sin\phi \\ \dfrac{\sin\theta}{\sin\phi} & -\dfrac{\cos\theta}{\sin\phi} & 0 \end{bmatrix}, \tag{7}$$

and

$$\mathbf{L}_{\boldsymbol{\omega}} = \begin{bmatrix} -\cos\theta & 0 \\ \dfrac{\sin\theta\cos\phi}{\sin\phi} & -1 \end{bmatrix}. \tag{8}$$

In (6),$(1/d)\mathbf{L}_v\boldsymbol{v}$ captures the translation motion part and $\mathbf{L}_\omega\boldsymbol{\omega}$ represents the rotation motion part. As $\boldsymbol{e}$ has only two components and the system has five inputs ($\boldsymbol{v}$ and $\boldsymbol{\omega}$), the control inputs are redundant for the controller design. To further simplify the SAA design, we assume v_x is constant and v_y and v_z are both zero. In other words, the host UAV flies with a constant forward speed during the entire SAA and $\boldsymbol{\omega}$ are the real inputs in our SAA design.

In long distance SAA, the rotation motion part dominates the feature error relative to the translation motion part [31], [32]. Thus, we set d to a worst value $d_{\min}$ and to avoid the use of the unknown d in (6). The translation motion part is then defined as

$$\mathbf{C}_v = \frac{1}{d_{min}}\mathbf{L}_v \boldsymbol{v}. \tag{9}$$

Although the avoidance maneuver efficiency is decreased with this treatment, we can solve the problem of lacking distance information.

From (6) and (9), the final controller of intruder avoidance maneuver is designed as

$$\boldsymbol{\omega}_1^c = -\mathbf{L}_{\boldsymbol{\omega}}^{-1}\left(\lambda_1 \boldsymbol{e} + \mathbf{C}_v\right) + \mathbf{L}_{\boldsymbol{\omega}}^{-1}\widehat{\frac{\partial \boldsymbol{e}}{\partial t}}, \tag{10}$$

where λ_1 is a controller parameter and $\mathbf{L}_\omega^{-1}$ is the inverse of $\mathbf{L}_w$, and $\widehat{\partial \boldsymbol{e}/\partial \boldsymbol{t}}$ is the output of the estimator of $\partial \boldsymbol{e}/\partial \boldsymbol{t}$.

In the following, we simply prove the convergence of the above controller design. We plug (10) into (6) to obtain

$$\dot{\boldsymbol{e}} = \frac{1}{d}\mathbf{L}_v \boldsymbol{v} - \mathbf{C}_v - \lambda_1 \boldsymbol{e} + \frac{\partial \boldsymbol{e}}{\partial t} - \widehat{\frac{\partial \boldsymbol{e}}{\partial t}}. \tag{11}$$

Let us define

$$\boldsymbol{r} = \frac{1}{d}\mathbf{L}_v \boldsymbol{v} - \mathbf{C}_v + \frac{\partial \boldsymbol{e}}{\partial t} - \widehat{\frac{\partial \boldsymbol{e}}{\partial t}}. \tag{12}$$

Since we consider long distance SAA, d and $d_{\min}$ are both relatively large, thus

$$\frac{1}{d}\mathbf{L}_v \boldsymbol{v} - \mathbf{C}_v = \frac{d - d_{\min}}{d d_{\min}}\mathbf{L}_v \boldsymbol{v} \approx 0. \tag{13}$$

Moreover, if the estimation of intruder state is accurate enough, we have $\partial e/\partial t - \widehat{\partial e/\partial t} \approx 0$. Thus, $\boldsymbol{r} \approx 0$ and (11) become

$$\dot{\boldsymbol{e}} = \lambda_1 \boldsymbol{e}. \tag{14}$$

Equation (14) indicates that the error will converge to $\mathbf{0}$ if λ_1 is chosen properly. Similar to [32], in case $\boldsymbol{r}$ does not approximate to zero and has residue, the error will converge towards $\boldsymbol{r}/\lambda_1$. Thus, setting a high λ_1 will help reduce the tracking error.

VISUAL SERVOING CONTROL FOR RETURNING MANEUVER

An avoidance maneuver is obtained by using the above visual servoing control. After the avoidance maneuver, the host UAV needs to return to $\mathcal{T}(t)$ The returning maneuver is triggered when the visual feature $\boldsymbol{s}$ reaches $\boldsymbol{s}^*$. To achieve the returning maneuver, the desired returning waypoint $\mathbf{P}^d \in \mathcal{T}(t)$ in $\mathcal{I}$ is first projected into $\mathcal{B}$,

$${}^{\mathcal{B}}\mathbf{P} = \mathbf{R}\left(\mathbf{P}^d - \mathbf{P}^c\right), \tag{15}$$

where $\mathbf{R}$ is the rotation matrix from $\mathcal{B}$ to $\mathcal{I}$, $\mathbf{P}^c$ is the current position of host UAV in $\mathcal{I}$. In visual servoing control, the desired destination waypoint is transformed to $q_d \coloneqq [\phi_d\ \theta_d]^T$ in $\mathcal{F}$, and

$$\begin{aligned} \phi_d &= \tan^{-1}\left(\frac{{}^{\mathcal{B}}\mathbf{P}_2}{{}^{\mathcal{B}}\mathbf{P}_1}\right), \\ \theta_d &= \tan^{-1}\left(\frac{{}^{\mathcal{B}}\mathbf{P}_3}{\sqrt{{}^{\mathcal{B}}\mathbf{P}_1^2 + {}^{\mathcal{B}}\mathbf{P}_1^2}}\right), \end{aligned} \tag{16}$$

where ${}^{\mathcal{B}}\mathbf{P}_1$, ${}^{\mathcal{B}}\mathbf{P}_2$, and ${}^{\mathcal{B}}\mathbf{P}_3$ are the three elements of ${}^{\mathcal{B}}\mathbf{P}$.

A visual servoing controller similar to (10) is proposed for the returning maneuver

$$\boldsymbol{\omega}_2^c = -\mathbf{L}_{\boldsymbol{\omega}}^{-1}\left(\lambda_2 \mathbf{q}_d + \frac{1}{d_c}\mathbf{L}_v \boldsymbol{v}\right), \tag{17}$$

where λ_2 is a controller parameter for the returning controller, and d_c is the distance between $\mathbf{P}^d$ and $\mathbf{P}^c$ that can be measured through the navigation system of the host UAV.

Table 1.

The SAA Parameters					
r_0 (rad)	r_{th} (rad)	ε_0 (rad)	ε_1 (rad)	λ_1	λ_2
0.1	0.35	0.01	0.2	–0.015	–0.02

Remark 4: *The dynamic safety envelope is still evolving during the returning maneuver. Thus,* $\boldsymbol{\omega}_2^c$ *may be switched back to* $\boldsymbol{\omega}_1^c$ *if the forward direction of the host UAV falls into the dynamic safety envelope again. The switching strategy is necessary for the proposed SAA approach. It is difficult to guarantee a successful avoidance by only one avoidance maneuver, because the avoidance strategy is only based on current and past vision information of the intruder and the future motion of the intruder is indeed unpredictable. The proposed visual servoing control is conservative and one maneuver is not sufficient in some time because of the lack of exact distance information. Therefore, it is this switching strategy that guarantees the effectiveness and completeness of the SAA.*

Remark 5: *In this article, we focus on the possibility of using a visual servoing controller to realize SAA without any distance measurement. No limitation of maneuverability is imposed on the controller design and we assume the commands from the visual servoing controller can be fully executed by the host UAV.*

SIMULATION RESULTS

The simulations were conducted to validate the proposed SAA approach. The values of the parameters used in the SAA are listed in Table 1. In the simulation, we used a kinematic model similar to [26] to verify the effectiveness of the visual servoing controller. The constant forward speed was set at 20 m/s and $d_{\min}$ was set 150 m in simulations.

In scenario 1, a head-on collision situation was simulated. The intruder and the host UAV were on same altitude level. Figure 5a demonstrates the real trajectories of the host UAV and the intruder.

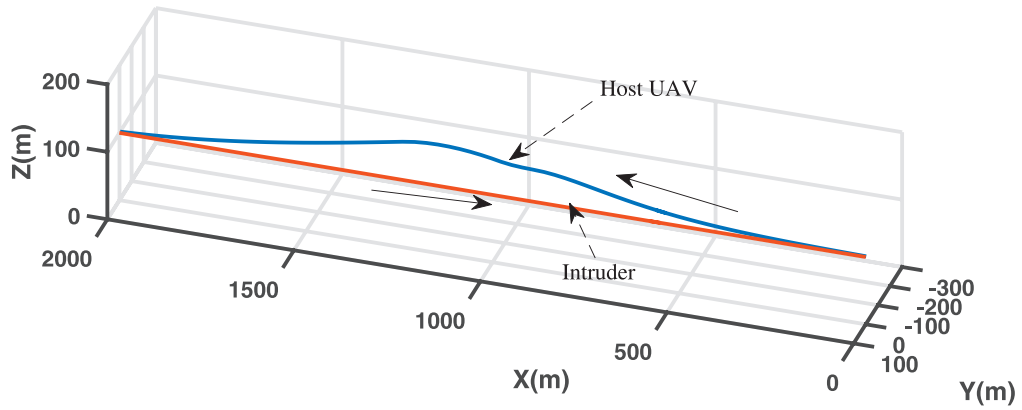

(a) 3D avoidance trajectories of simulation scenario 1

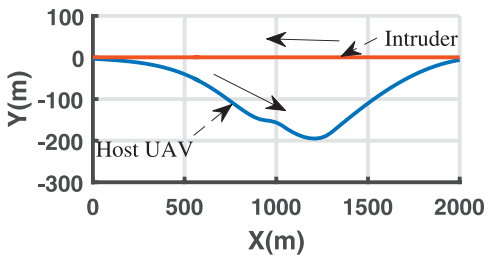

(b) Avoidance trajectories on XY plane

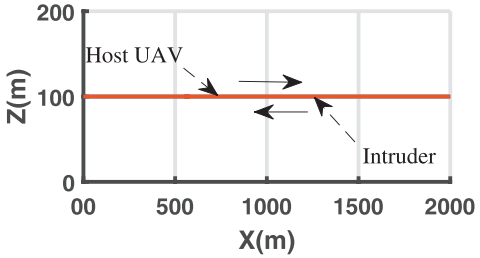

(c)Avoidance trajectories on XZ plane

Figure 5.
Real avoidance trajectories of simulation scenario 1.

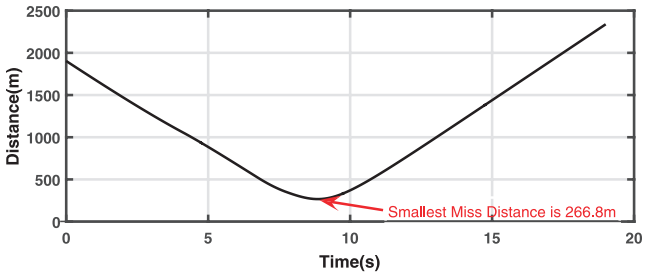

Figure 6.
The separation distance in scenario 1.

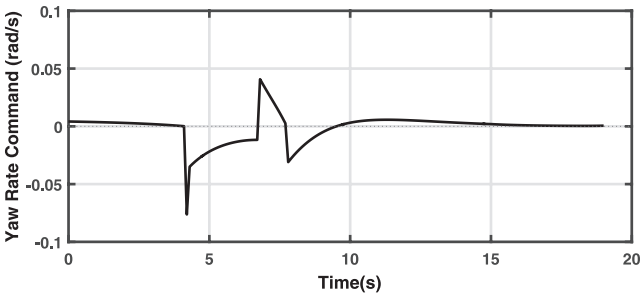

Figure 7.
The controller output of yaw angle rate in scenario 1. The avoidance maneuver started at 4.1 s and ceased at 9.7 s.

Figure 5b and Figure 5c show the projections of the real trajectories onto the *XY*-plane and *XZ*-plane, respectively. It is clear that the host UAV successfully avoided the intruder and returned to the desired trajectory. Figure 6 shows that the minimum separation distance between the host UAV and the intruder is about 268 m during the SAA. The output of the servoing controller is presented in Figure 7. At the same altitude, the controller of host UAV only has yaw angle command to the autopilot.

In scenario 2, a cross collision situation was investigated. The trajectories of the host UAV and the intruder were shown in Figures 8a, 8b, 8c. Again, the results showed that the host UAV was able to implement an effective maneuver to avoid the intruder. Fig-

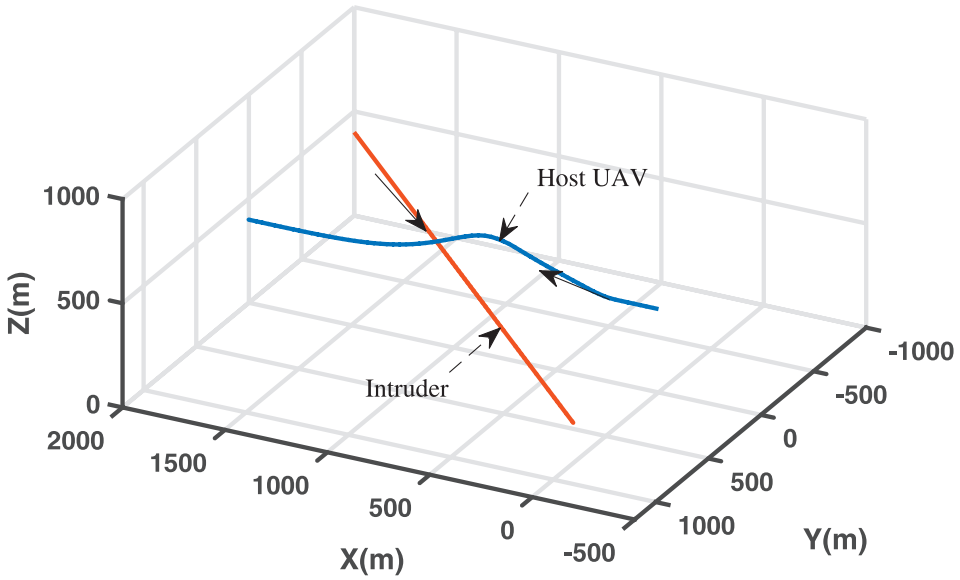

(a) 3D avoidance trajectories of simulation scenario 2

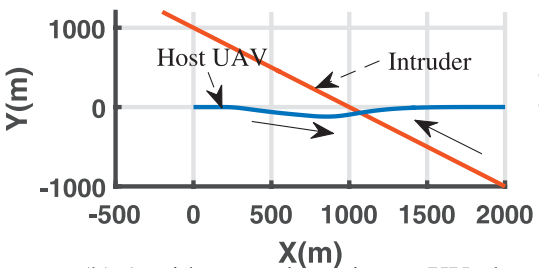

(b) Avoidance trajectories on XY plane

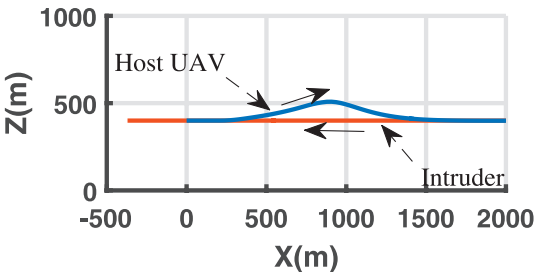

(c) Avoidance trajectories on XZ plane

Figure 8.
Real avoidance trajectories of simulation scenario 2.

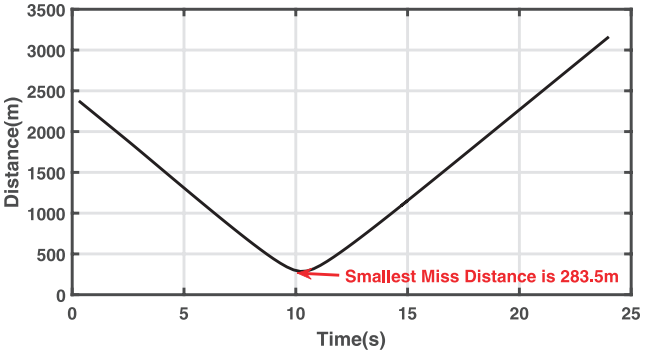

Figure 9.
The separation distance in scenario 1.

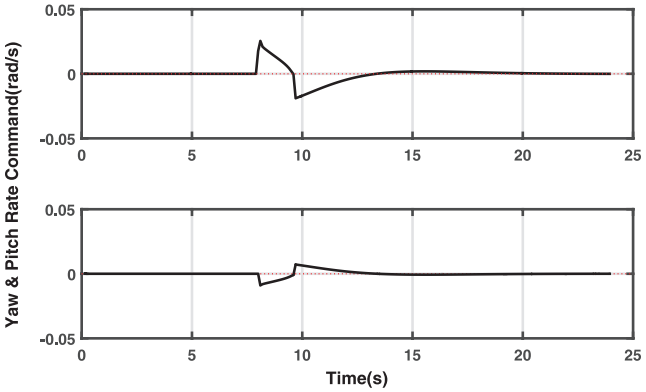

Figure 10.
The controller outputs in scenario 2 (the top plot for yaw angle rate and the bottom plot for pitch angle rate). The avoidance maneuver started at 7.9 s and ceased at 13.7 s.

ure 9 presents a 284 m minimum separation distance. In this case, the host UAV executes yaw and pitch motion maneuvers simultaneously as shown in Figure 10. These simulation results show that the proposed vision-based SAA can achieve effective SAA in different situations.

EXPERIMENTAL RESULTS

Figure 11 shows the experiment setup used in the study. The small rotorcraft (Model 700N from TREX corporation, Taiwan) was used as the host UAV; see Figure 11a. The camera (GoPro Type with 110° × 70° FOV angle) was mounted on the head of the

Ground Control receives image detection results from the UAV, executes the SAA algorithm, and transmits commands for the avoidance maneuver back to the autopilot.

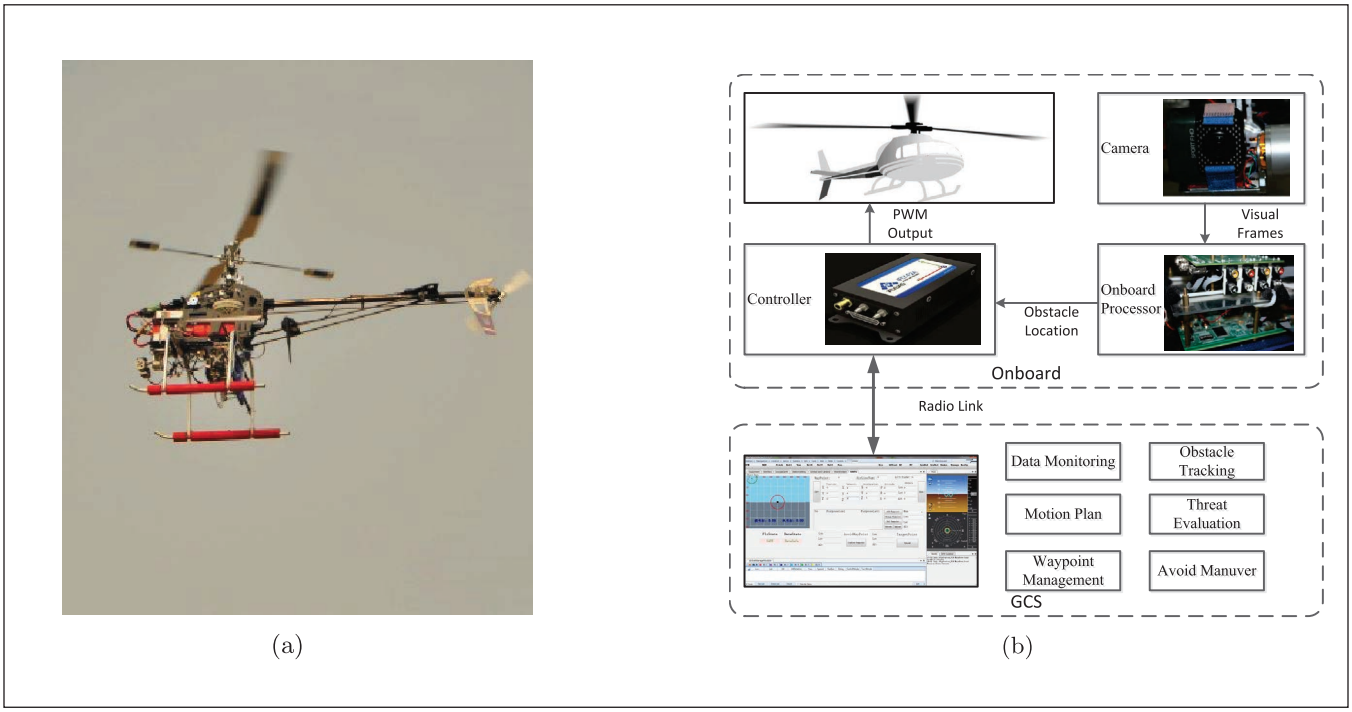

Figure 11.
The developed SAA experiment setup.

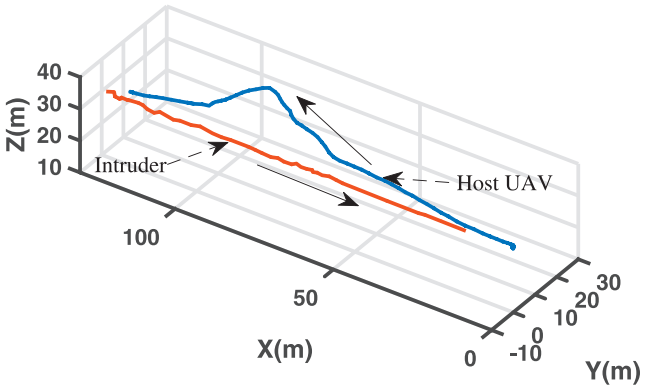

(a)The 3D avoidance trajectories in experiment

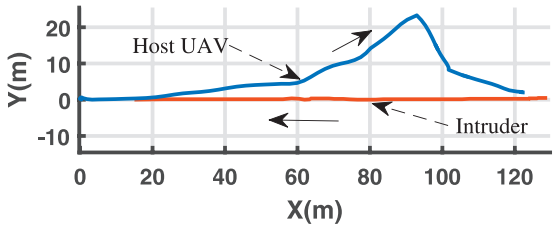

(b)The avoidance trajectories projected on XY plane

Figure 12.
Real avoidance trajectories in the experiment.

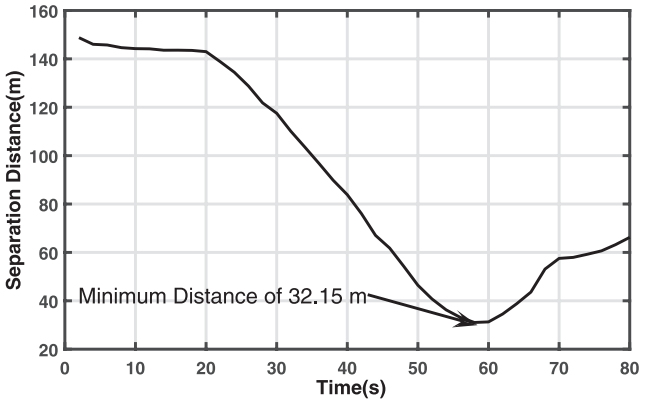

Figure 13.
The separation distance in the experiment.

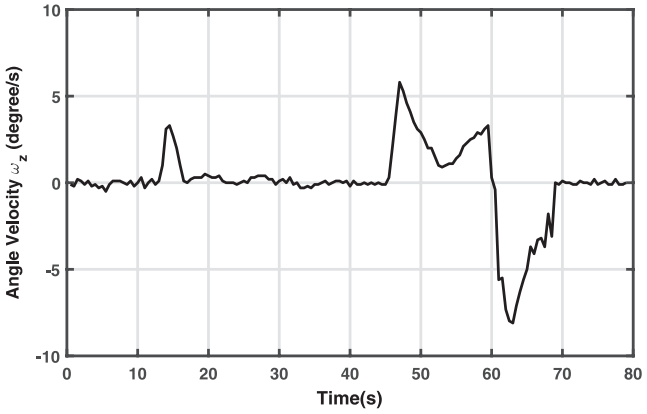

Figure 14.
The controller output of yaw angle rate in the experiment.

rotorcraft. The experiment setup was designed for airborne SAA, but for safety considerations, we ran the proposed SAA approach using Ground Control Station (GCS). Image detection was processed by an onboard DM8168 Digital Signal Processor. The GCS received the detection results through a down-radio-link and executed the proposed SAA algorithm. The feedback angle velocity commands of the avoidance maneuver were then transmitted back to the autopilot through up-radio-link; see Figure 11b. A hexrotor UAV with 60 cm diameter were operated manually as the intruder. Due to the limitations of the hardware, the work frequency of the SAA was at 10 Hz. The linear forward velocity of the host UAV was set at 2 m/s during the experiment. The intruder flies with a speed 1.5 m/s towards the host UAV. $d_{\min}$ was set as 15 m in experiment.

A head-on experiment was conducted to validate the proposed approach. Figure 12 shows the real trajectories of the host UAV and the intruder. We omit the projections of the real trajectories onto *XZ*-plane because the host UAV and intruder are almost at the same altitude during the SAA, similar to simulation scenario 1. The relative distance between host UAV and intruder is presented in Figure 13 with a minimum separation distance of 32.15 m. Figure 14 shows the yaw angle velocity commands to the autopilot. Three snapshots taken from the ground are shown in Figure 15 to further illustrate the experiment. In Figure 15a, the intruder was initially detected by the host UAV. In Figure 15b, the host UAV conducted collision avoidance maneuver according to the envelope evolution. Finally, the host UAV returned to its original path in Figure 15c. Figure 16 shows how the dynamic safety envelope changed during the experiment. $\mathcal{L}_1 - \mathcal{L}_5$ represents five envelopes at different time. $\mathcal{L}_1$ is the initial envelope. $\mathcal{L}_2$ is the envelope when the host UAV starts the avoidance maneuver. $\mathcal{L}_3 - \mathcal{L}_5$ shows the envelopes during avoidance. It is clear that the forward direction leaves $\mathcal{L}_3$ under the servoing controller. For $\mathcal{L}_4$ and $\mathcal{L}_5$, the forward direction moves in and out of the envelope due to switching between the avoidance and returning controllers. The dash-line represents the trajectory of q (the intruder).

CONCLUSION

In this article, a vision-only based collision avoidance approach was proposed for SAA of UAVs. The 2D dynamic safety envelope was first generated to capture the threat level of the non-cooperative flying intruder and guide avoidance. Two visual servoing controllers were then designed to separately implement the avoidance and the returning maneuvers. The proposed collision avoidance approach does not require distance information. We demonstrated the effectiveness of the approach through simulations and experiments.

We are currently conducting additional tests with additional scenarios. Additionally, we are investigating collision avoidance approach for multiple intruders.

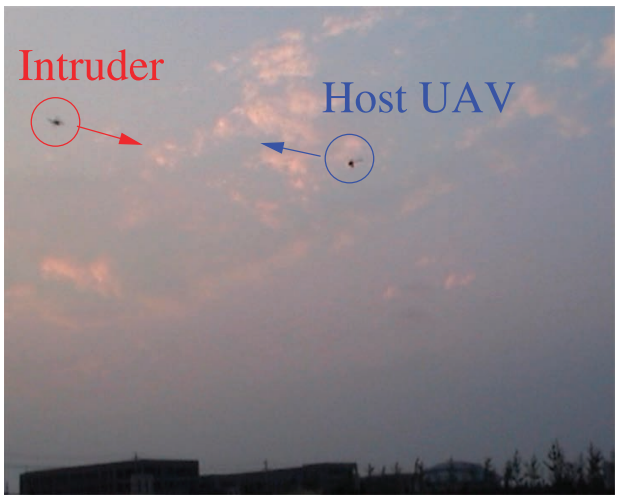

(a)

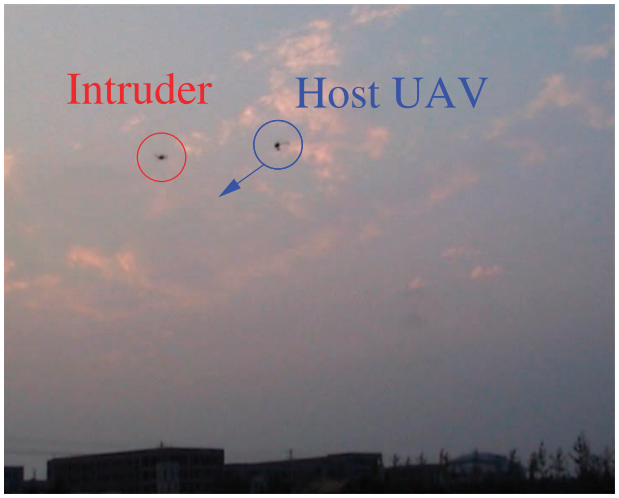

(b)

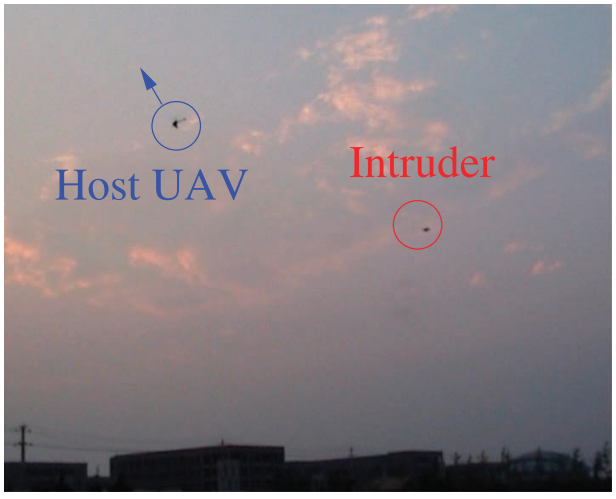

(c)

Figure 15.
Snapshots of the SAA experiment.

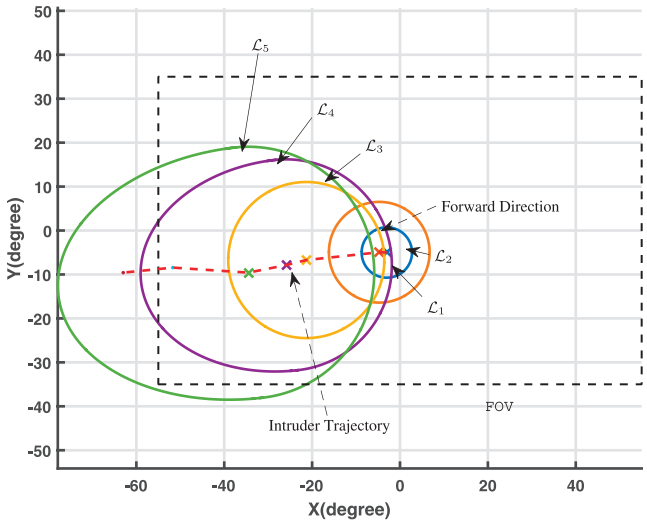

Figure 16.
Envelope evolution in the experiment.

ACKNOWLEDGEMENTS

The authors are grateful to Brad Yu at Australian National University for his helpful discussions and suggestions. The authors also thank Haifeng Zhu and Tongguo Tang at Northwestern Polytechnical University for their efforts with the experiments and simulations.

REFERENCES

[1] Mystkowski, A. Implementation and investigation of a robust control algorithm for an unmanned micro-aerial vehicle. *Robotics and Autonomous Systems*, Vol. 62, 8 (2014), 1187–1196.

[2] Chowdhary, G., Johnson, E. N., Magree, D., Wu, A., and Shein, A. GPS-denied indoor and outdoor monocular vision aided navigation and control of unmanned aircraft. *Journal of Field Robotics*, Vol. 30, 3 (2013), 415–438.

[3] Huh, S., Shim, D., and Kim, J. Integrated navigation system using camera and gimbaled laser scanner for indoor and outdoor autonomous flight of UAVs. In *Proceedings of the IEEE/RSJ International Conference on Intelligent Robots and Systems*, Tokyo, Japan, 2013, 3158–3163.

[4] Moses, A., Rutherford, M. J., Kontitsis, M., and Valavanis, K. P. UAV-borne X-band radar for collision avoidance. *Robotica*, Vol. 32, 1 (2014), 97–114.

[5] Nigam, N., Bieniawski, S., Kroo, I., and Vian, J. Control of multiple UAVs for persistent surveillance: algorithm and flight test results. *IEEE Transactions on Control Systems Technology*, Vol. 20, 5 (2012), 1236–1251.

[6] Gurtner, A., Greer, D. G., Glassock, R., Mejias, L., Walker, R., Boles, W. W., et al. Investigation of fish-eye lenses for small-UAV aerial photography. *IEEE Transactions on Geoscience and Remote Sensing*, Vol. 47, 3 (2009), 709–721.

[7] Bernard, M., Kondak, K., Maza, I., and Ollero, A. Autonomous transportation and deployment with aerial robots for search and rescue missions. *Journal of Field Robotics*, Vol. 28, 6 (2011), 914–931.

[8] Angelov, P. *Sense and Avoid in UAS: Research and Applications*. John Wiley & Sons, 2012.

[9] Lee, H.-C. Implementation of collision avoidance system using TCAS II to UAVs. *IEEE Aerospace and Electronic Systems Magazine*, Vol. 21, 7 (2006), 8–13.

[10] Stark, B., Stevenson, B., and Chen, Y. ADS-B for small unmanned aerial systems: Case study and regulatory practices. In *Proceedings of the International Conference on Unmanned Aircraft Systems*, 2013, 152–159.

[11] Lai, J., Mejias, L., and Ford, J. J. Airborne vision-based collision-detection system. *Journal of Field Robotics*, Vol. 28, 2 (2011), 137–157.

[12] Kwag, Y., and Chung, C. UAV based collision avoidance radar sensor. In *Proceedings of the IEEE International Geoscience and Remote Sensing Symposium*, 2007, 639–642.

[13] Chamberlain, L. J., Scherer, S., and Singh, S. Self-aware helicopters: Full-scale automated landing and obstacle avoidance in unmapped environments. *AHS Forum 67*, 2011.

[14] Fasano, G., Accardo, D., Moccia, A., Carbone, C., Ciniglio, U., Corraro, F., et al. Multi-sensor-based fully autonomous non-cooperative collision avoidance system for unmanned air vehicles. *Journal of Aerospace Computing, Information, and Communication*, Vol. 74, (2008), 338–360.

[15] Yu, X., and Zhang, Y. Sense and avoid technologies with applications to unmanned aircraft systems: Review and prospects. *Progress in Aerospace Sciences*, Vol. 74, (2015), 152–166.

[16] Frazzoli, E., Dahleh, M., Feron, E., et al. Real-time motion planning for agile autonomous vehicles. In *Proceedings of the American Control Conference*, *Vol. 1*, 2001, 43–49.

[17] Kim, Y., Gu, D.-W., and Postlethwaite, I. Real-time path planning with limited information for autonomous unmanned air vehicles. *Automatica*, Vol. 44, 3 (2008), 696–712.

[18] Lai, J., Ford, J. J., Mejias, L., and OŚhea, P. Characterization of sky-region morphological-temporal airborne collision detection. *Journal of Field Robotics,* Vol. 30, 2 (2013), 171–193.

[19] May, K., and Krouglicof, N. Moving target detection for sense and avoid using regional phase correlation. In *Proceedings of the IEEE International Conference on Robotics and Automation*, 2013, 4,767–4,772.

[20] Fasano, G., Accardo, D., Tirri, A. E., Moccia, A., and Lellis, E. D. Sky region obstacle detection and tracking for vision-based UAS sense and avoid. *Journal of Intelligent and Robotic Systems,* (2015), 1–24.

[21] Zarandy, A., Nagy, Z., Vanek, B., Zsedrovits, T., Kiss, A., Nemeth, M. A five-camera vision system for UAV visual attitude calculation and collision warning. In *Computer Vision Systems*, Vol. 7,963, Springer Berlin Heidelberg, 2013, pp. 11–20.

[22] Griffiths, S., Saunders, J., Curtis, A., Barber, B., McLain, T., Beard, R. Maximizing miniature aerial vehicles—obstacle and terrain avoidance for MAVs. *IEEE Robotics and Automation Magazine*, Vol. 13, 3 (2006), 34–43.

[23] Vanek, B., Peni, T., Bokor, J., Zsedrovits, T., Zarandy, A., and Roska, T. Performance analysis of a vision only sense and avoid system for small UAVs. In *Proceedings of the AIAA Guidance, Navigation, and Control Conference,* 2013, 4,767–4,772.

[24] Yang, X., Alvarez, L. M., and Bruggemann, T. A 3D collision avoidance strategy for UAVs in a non-cooperative environment. *Journal of Intelligent and Robotic Systems*, Vol. 70, 1–4, SI (2013), 315–327.

[25] Mcfadyen, A., Mejias, L., Corke, P., and Pradalier, C. Aircraft collision avoidance using spherical visual predictive control and single point features. In *Proceedings of the IEEE/RSJ International Conference on Intelligent Robots and Systems*, 2013, 50–56.

[26] Choi, H., Kim, Y., and Hwang, I. Reactive collision avoidance of unmanned aerial vehicles using a single vision sensor. *Journal of Guidance Control Dynamics*, Vol. 36, 4 (2013), 1,234–1,240.

[27] Nordlund, P. J., and Gustafsson, F. Probabilistic noncooperative near mid-air collision avoidance. *IEEE Transactions on Aerospace and Electronic Systems,* Vol. 47, 2 (2011), 1,265–1,276.

[28] Mcfadyen, A., Corke, P., and Mejias, L. Rotorcraft collision avoidance using spherical image-based visual servoing and single point features. In *Proceedings of the IEEE/RSJ International Conference on Intelligent Robots and Systems*, 2012, 1,199–1,205.

[29] Angelov, P., Bocaniala, C. D., Xideas, C., Patchett, C., Ansell, D., Everett, M., et al. A passive approach to autonomous collision detection and avoidance in uninhabited aerial systems. In *Proceedings of the International Conference on Computer Modeling. and Simulation*, 2008, 64–69.

[30] Tadema, J., Theunissen, E., and Kirk, K. Self-separation support for UAS. In *Proceedings of the AIAA Infotech@Aerospace Conference*, 2010.

[31] Chaumette, F., and Hutchinson, S. Visual servo control I: Basic approaches. *IEEE Robotics and Automation Magazine*, Vol. 13, 4 (2006), 82–90.

[32] Chaumette, F., and Hutchinson, S. Visual servo control II: Advanced approaches. *IEEE Robotics and Automation Magazine*, Vol. 14, 1 (2007), 109–118.